CrossMark

J. Fluid Mech. (2005), *vol.* 522, *pp.* 35–62. © 2005 Cambridge University Press
DOI: 10.1017/S0022112004001351 Printed in the United Kingdom

Rotating gravity currents. Part 1. Energy loss theory

By J. R. MARTIN[1]† AND G. F. LANE-SERFF[2]

[1]School of Ocean & Earth Science, Southampton Oceanography Centre, University of Southampton, Waterfront Campus, European Way, Southampton SO14 3ZH, UK

[2]Manchester Centre for Civil and Construction Engineering, UMIST, PO Box 88, Manchester M60 1QD, UK
g.f.lane-serff@umist.ac.uk

(Received 17 January 2003 and in revised form 21 July 2004)

A comprehensive energy loss theory for gravity currents in rotating rectangular channels is presented. The model is an extension of the non-rotating energy loss theory of Benjamin (*J. Fluid Mech.* vol. 31, 1968, p. 209) and the steady-state dissipationless theory of rotating gravity currents of Hacker (PhD thesis, 1996). The theory assumes the fluid is inviscid, there is no shear within the current, and the Boussinesq approximation is made. Dissipation is introduced using a simple method. A head loss term is introduced into the Bernoulli equation and it is assumed that the energy loss is uniform across the stream. Conservation of momentum, volume flux and potential vorticity between upstream and downstream locations is then considered. By allowing for energy dissipation, results are obtained for channels of arbitrary depth and width (relative to the current). The results match those from earlier workers in the two limits of (i) zero rotation (but including dissipation) and (ii) zero dissipation (but including rotation). Three types of flow are identified as the effect of rotation increases, characterized in terms of the location of the outcropping interface between the gravity current and the ambient fluid on the channel boundaries. The parameters for transitions between these cases are quantified, as is the detailed behaviour of the flow in all cases. In particular, the speed of the current can be predicted for any given channel depth and width. As the channel depth increases, the predicted Froude number tends to $\sqrt{2}$, as for non-rotating flows.

1. Introduction

1.1. *Background*

Gravity (or density) currents are flows along a lower or upper boundary driven by density contrasts. The fluid in the gravity current has a different density from the surrounding ambient fluid, resulting from differences in temperature or composition, or from suspended particles. There are many examples in the natural and built environment, including sea breezes, fresh river water flowing into the sea, cool air flowing into a room, dense gas releases, turbidity currents and avalanches. A general review of gravity currents (in the absence of rotation effects) is given by Simpson (1982, 1997). The main features of a two-dimensional, non-rotating gravity current

† Present affiliation: Southampton University Hospitals NHS Trust, Mail Point 79, Southampton General Hospital, Tremona Road, Southampton SO16 6YD, UK; jrmartin2@ntlworld.com

https://doi.org/10.1017/S0022112004001351 Published online by Cambridge University Press

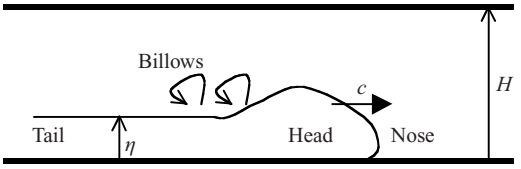


FIGURE 1. Sketch of a two-dimensional, non-rotating gravity current, following a rectangular channel of finite depth.

flowing along a horizontal surface are sketched in figure 1. The characteristic features include a raised 'head' at the front of the flow with a shallower 'tail' behind. The region towards the rear of the head often has Kelvin–Helmoltz billows, which cause some mixing between the gravity current and ambient fluid. However, it is common to treat the fluids as immiscible to simplify the theoretical treatment.

A theoretical analysis for a gravity current in a (non-rotating) rectangular channel is given by Benjamin (1968). For these flows we will denote the depth of the gravity current by η (height of tail, not head), the total depth of the channel by H, the speed of the current by c, the density of the ambient fluid by ρ and the density of the gravity current by $\rho + \Delta\rho$. We will assume that the density contrast is relatively small so that the Boussinesq approximation can be made and we define the 'reduced gravity' by

$$g' = g(\Delta\rho/\rho), \tag{1.1}$$

where g is the acceleration due to gravity. The speed of the gravity current is often represented in terms of a Froude number,

$$Fr = c/\sqrt{g'\eta}. \tag{1.2}$$

Benjamin showed that for a flow without energy dissipation, the current must occupy half the depth of the channel (i.e. $\eta = H/2$). Gravity currents of this type may be created by lock-exchange experiments, created by completely removing a vertical barrier separating two volumes of fluid of different density. These half-depth currents do not have the characteristic head or billows shown in figure 1 and their speed is predicted to be given by $Fr = 1/\sqrt{2}$. For flows with dissipation, Benjamin shows that the gravity current must occupy less than half the depth, with $Fr \to \sqrt{2}$ as $H \to \infty$. In experiments with $\eta < H/2$ gravity currents of the form sketched in figure 1 are found, though the Froude number is limited to a value of approximately $Fr = 1.1$ as H becomes very large (e.g. Lane-Serff, Beale & Hadfield 1995). Benjamin's theoretical approach is considered in more detail in § 2.

In a rotating system, the release of a dense fluid results in a gravity current that initially spreads in a similar fashion to the non-rotating case. After a time that scales with the rotation period the effects of rotation give a flow perpendicular to the initial flow direction. Where the current is constrained by lateral boundaries a jet forms parallel to the boundary and is held against it by Coriolis forces normal to the direction of flow. The width to which the flow adjusts scales with the Rossby radius of deformation, $R = (g'\eta)^{1/2}/f$, where g' is again the reduced gravity, η the depth and f the Coriolis parameter (Rossby 1938). Much of the existing work on rotating gravity currents considers currents flowing against a straight boundary in an ambient fluid that is effectively unbounded in depth and width; see the review by Griffiths (1986).

Stern, Whitehead & Hua (1982) presented a theoretical model of rotating gravity currents based on laboratory observations and earlier work (Stern 1980). They found

https://doi.org/10.1017/S0022112004001351 Published online by Cambridge University Press

that the theoretical nose speed was unaffected by the fractional depth of the current whereas in the non-rotating case Benjamin (1968) found that there was a strong dependence on the finite depth of the lower layer. Nof (1987) criticised the use of the long-wave equations in Stern's theory, since the current is non-hydrostatic in the nose region and instead used a similar method to Benjamin, applying conservation of energy, momentum and continuity to a control volume connecting the flow behind and ahead of the nose. His model includes a free surface and considers a current of wedge-like cross-section, with zero potential vorticity and finite depth.

Hacker (1996) and Hacker & Linden (2002) used a similar approach to Nof, applying conservation of momentum, energy, volume flux and potential vorticity. However they did not assume zero potential vorticity and introduced a rigid lid. The governing equations describing the structure of the flow were applied to three flow geometries, based on the width of the current as the rotation rate increases. For each case a solution was found for the speed of the current. Hacker successfully avoided the hydrostatic problem and provided a steady solution for all levels of rotation, with a smooth progression between the non-rotating and weakly rotating case. Nof's solutions can be compared with Hacker's solutions for intermediate rotation rate and, despite the inclusion of a free surface and the assumption of zero potential vorticity in Nof's analysis, the results compare quite well. Hacker's theory does not include dissipation or the effect of the potential vorticity distribution at the source region on the resulting flow, but we use it as the starting point for our theory.

1.2. *Overview*

The present work consists of two papers. In this paper (Part 1), we develop a theory which allows us to find theoretical results for rotating gravity currents in rectangular channels of arbitrary relative width and depth (compared to the gravity current). In the second paper (Martin, Smeed & Lane-Serff 2004) we take a different approach, allowing for uniform potential vorticity within the gravity current (though no energy dissipation). This approach gives insights into flows in which there is a shear across the current.

Returning to the present paper, in § 2 we review the theoretical background in more detail, concentrating on the dissipative non-rotating theory of Benjamin (1968) and the non-dissipative but rotating theory of Hacker (1996). In § 3 we develop a comprehensive theory for rotating gravity currents including energy dissipation. The detailed results are presented and discussed in § 4, and we draw some conclusions and identify areas for further study in § 5.

2. Theoretical background

The theory we develop in § 3 effectively 'fills in' the parameter space between the non-rotating, dissipative theory of Benjamin (1968) and the rotating, energy-conserving theory of Hacker (1996) and Hacker & Linden (2002). Here we give some of the main results from the earlier theories, and derive those basic results that apply to the earlier theories and still apply in our more comprehensive theory.

2.1. *Non-rotating gravity currents*

Non-rotating theory

Benjamin's model of a gravity current considers the analogous flow of a steady inviscid fluid of density ρ past a cavity (figure 2). The cavity may be filled with fluid of negligible density (such as air) or empty. The flow is confined between two horizontal

https://doi.org/10.1017/S0022112004001351 Published online by Cambridge University Press

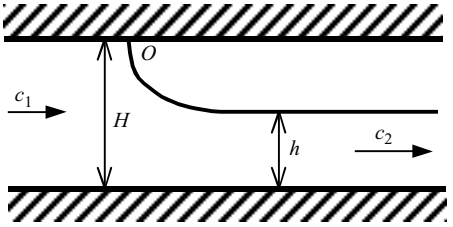


FIGURE 2. Benjamin's (1968) model of flow of an inviscid fluid past a cavity of air.

planes. The pressure at the free surface is taken as zero. Upstream the fluid has depth, H, and propagates at a constant velocity, c_1. Beneath the cavity far downstream the flow is uniform with depth, h, and constant velocity, c_2.

Benjamin obtains an expression for c_2 by applying the Bernoulli equation along a streamline connecting the stagnation point and a point downstream on the free surface, giving

$$c_2^2 = 2g(H-h), \tag{2.1}$$

and shows that for energy-conserving flow the fluid must occupy half the depth of the channel,

$$h = \tfrac{1}{2}H, \quad \text{with} \quad c_1/(gH)^{1/2} = \tfrac{1}{2} \quad \text{and} \quad c_2/(gH)^{1/2} = \sqrt{2}. \tag{2.2}$$

Benjamin (1968) conjectures that in order to allow different rates of flow, dissipation must occur, through the fluid experiencing a uniform loss of total head. The head loss term, Δe, is incorporated into the Bernoulli equation (2.1) to give,

$$c_2^2 = 2g(H-h-\Delta e). \tag{2.3}$$

Using conservation of momentum together with (2.3) we can find an expression for Δe,

$$\Delta e = \frac{(2h-H)(H-h)^2}{2h(2H-h)}. \tag{2.4}$$

Equation (2.4) confirms that the energy-conserving depth is $h = \frac{1}{2}H$. Energy loss is possible when h is greater than this depth. Depths less than the dissipationless depth are unlikely, as these would require a gain in energy. We can find expressions for the speed of the flow,

$$\frac{c_1}{\sqrt{gH}} = \frac{\sqrt{h(H^2-h^2)}}{\sqrt{H^2(2H-h)}}, \tag{2.5}$$

and the total flow rate (per unit width),

$$\frac{Q}{\sqrt{gH^3}} = \frac{\sqrt{(H-h)^2h(H^2-h^2)}}{\sqrt{H^4(2H-h)}}. \tag{2.6}$$

The Froude number based on the propagation rate of the cavity reveals that for shallow currents as $(H-h)/H$ tends to zero the Froude number $(c_1/(g(H-h))^{1/2})$ tends to $\sqrt{2}$.

2.2. *Rotating gravity currents*

Model description

As in Hacker (1996), the model is based on three flow geometries as the rotation rate is increased (figure 3). In case A, 'weak rotation', the current fills the full width

https://doi.org/10.1017/S0022112004001351 Published online by Cambridge University Press

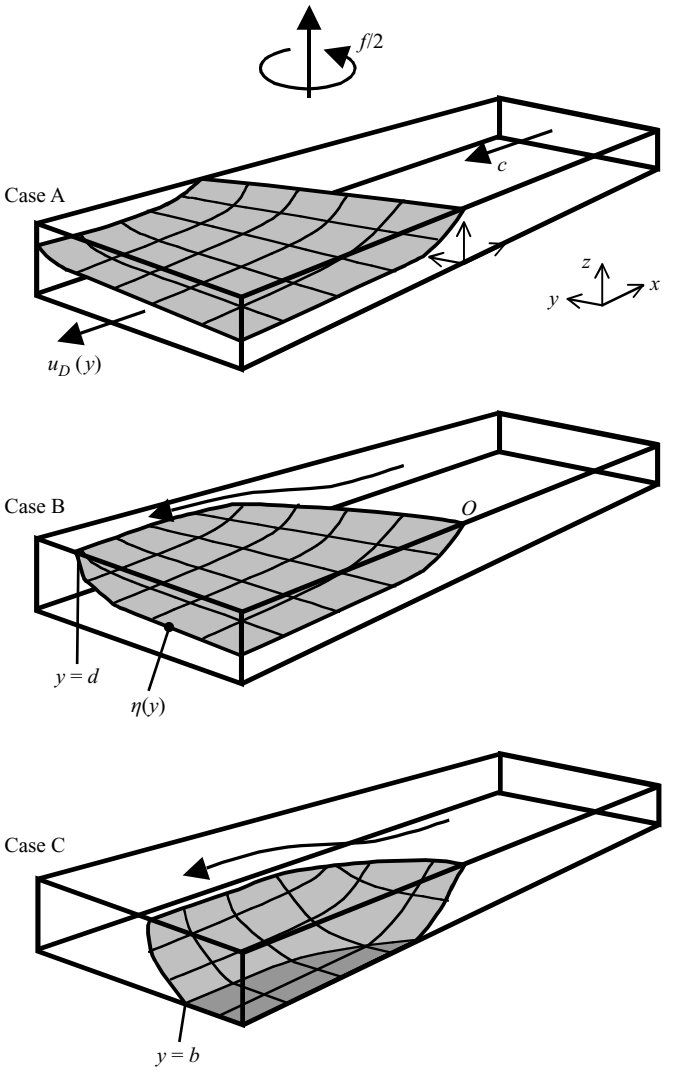


FIGURE 3. Flow geometries for the three levels of background rotation in the steady reference frame. The surface gravity current is shaded whilst the ambient fluid is clear. Upstream in the ambient fluid there is no flow. The interface between the current and ambient fluid propagates at speed c parallel to the channel walls and floor. Hence, the gravity current appears stationary to an observer moving with the current, whilst the oncoming ambient fluid has speed c. This is known as the steady reference frame. (a) Case A (low rotation) – current fills the full width of the channel. (b) Case B (moderate rotation) – current outcrops on the upper boundary at $y = d$. (c) Case C (strong rotation) – current outcrops on the upper boundary and fills the full depth of the channel, intersecting the bottom boundary at $y = b$. (Adapted from Hacker 1996).

of the channel. In case B the current detaches from the left-hand wall and outcrops on the free surface, at position d. For stronger rotation rates, case C, the current fills the full depth of the channel, outcropping on the bottom of the tank at position b.

The model considers a surface gravity current. The interface of the current propagates at a constant speed c. The reference frame is rotating at angular frequency $f/2$ and translating at speed c, hence the gravity current appears stationary. Within the current there is no flow. The role of the current is merely to produce the pressure

https://doi.org/10.1017/S0022112004001351 Published online by Cambridge University Press

gradient necessary to drive the flow in the ambient fluid. There is no mixing between the two fluids. Downstream the flow in the gravity current is parallel to the walls and floor. The channel has a rigid lid and the Boussinesq approximation is made.

Redefinition of variables

The parameters and variables in the model are defined as follows. The dimensional variables are marked with an asterisk. Vectors are in bold type. The subscripts c and a refer to the current and ambient fluid respectively, with U the upstream and D the downstream locations. The subscript 0 specifies a variable measured at the right-hand wall, which is therefore a constant. Where a symbol appears only once, it is defined in the text.

The reduced gravity is given by $g' = g\Delta\rho/\rho_a$ where $\Delta\rho = \rho_a - \rho_c$, the channel width is D, the channel depth H, and the Coriolis parameter f. We define a Rossby radius in terms of the total channel depth $R = f/(g'H)^{1/2}$. The aspect ratio of the channel is denoted by $\lambda_H = H/D$, and we also define a density ratio $\rho = \rho_c^*/\rho_a^* = 1 - \Delta\rho^*/\rho_a^*$. For Boussinesq flow we can take $\rho = 1$. We non-dimensionalize distances and speeds as follows:

$$\left.\begin{array}{lll} \text{horizontal lengths} & x = x^*/D, & y = y^*/D, \\ \text{vertical lengths} & z = z^*/H, & \eta = \eta^*/H, \\ \text{velocities} & \boldsymbol{u} = \boldsymbol{u}^*/(g'H)^{1/2}, & \\ \text{velocity of the leading edge} & c = c^*/(g'H)^{1/2}, & \\ \text{pressure} & p = (p^* - \rho_a^* g z^*)/(\rho_a^* g' H). & \end{array}\right\} \tag{2.7}$$

Note that in addition to scaling the pressure term we also remove a hydrostatic component. An important parameter is the strength of the rotation: this is characterized by the ratio of the width of the channel to the Rossby radius of deformation, $W = fD/(g'H)^{1/2}$.

Basic equations

Momentum equation

The non-dimensional form of the momentum equation for the current is

$$\rho \boldsymbol{u}_C \cdot \nabla \boldsymbol{u}_C + \rho W(\boldsymbol{k} \times \boldsymbol{u}_C) = -\nabla p_C - \rho W c \boldsymbol{j} + \lambda_H^{-1} \boldsymbol{k}, \tag{2.8}$$

where the second term on the right-hand side is the Coriolis force experienced by the frame of reference and is known as the 'body force of translation'. It is a result of the change from the steady rest frame to a reference frame translating at the speed c. The momentum equation for the ambient fluid is

$$\boldsymbol{u}_a \cdot \nabla \boldsymbol{u}_a + W(\boldsymbol{k} \times \boldsymbol{u}_a) = -\nabla p_a - W c \boldsymbol{j}. \tag{2.9}$$

Clearly the solution will depend on the size of the parameter W.

Geostrophic equations

Far upstream and downstream of the current head, we assume that the flow is parallel to the channel walls so that we can write

$$\boldsymbol{u}_c = (u_c(y, z), 0, 0), \tag{2.10}$$

$$\boldsymbol{u}_a = (u_a(y, z), 0, 0). \tag{2.11}$$

Note that we expect u_a to be negative. The non-dimensionalized momentum equations (2.8) and (2.9) are decomposed into x-, y- and z-components making use of (2.10)

https://doi.org/10.1017/S0022112004001351 Published online by Cambridge University Press

and (2.11) and hence the geostrophic relationships for the current

$$\frac{\partial p_c}{\partial y} = -\rho W(u_c + c) \tag{2.12}$$

and the ambient fluid

$$\frac{\partial p_D}{\partial y} = -W(u_D + c) \tag{2.13}$$

are obtained. The subscript D refers to the ambient fluid downstream.

Across-stream pressure

To determine the pressure for the current the velocity, v_c, is set to zero in (2.12). This enables the geostrophic equation to be integrated easily using the boundary condition that the pressure is zero at the foremost stagnation point $(0, 0, 1)$. At this stage in the calculation the Boussinesq approximation is made, $\rho = 1$:

$$p_c = (z - 1) - Wcy \tag{2.14}$$

By applying (2.13) to the ambient fluid upstream where the velocity $u_U = -c$, the pressure becomes a constant, hence

$$p_U = p_0. \tag{2.15}$$

In the ambient fluid downstream the pressure is set by that of the current at the interface, $z = 1 - \eta$, because the hydrostatic pressure variation in the ambient fluid has been removed, so (2.14) becomes

$$y \in [0, d]: \quad p_D = -\eta(y) - Wcy. \tag{2.16}$$

To obtain the pressure in the free stream around the current, the geostrophic equation (2.13) is integrated using the boundary condition that at

$$y = d: \quad p_D(d) = -Wcd,$$

hence

$$y \in [d, 1]: \quad p_D(y) = -WU_D(y - d) - Wcy. \tag{2.17}$$

Conservation of potential vorticity

Potential vorticity is materially conserved between the upstream and downstream locations in the ambient fluid where the flow is hydrostatic. We show later that even for flows with energy dissipation, potential vorticity can still be conserved in certain cases and so it is worthwhile to use this assumption in our analysis. Non-dimensionalizing the shallow-water potential vorticity and applying conservation of potential vorticity between up- and downstream gives

$$\mathrm{d}u_D/\mathrm{d}y = W\eta. \tag{2.18}$$

Flow structure equations

The structure of the flow is defined in terms of its depth, η_0, and the velocity at the right-hand wall of the channel, u_0. The general solutions for the across-stream depth $\eta(y)$ and velocity $u(y)$ are applicable for the whole of case A, and for $y \in [0, d]$ in case B. In the free stream around the current in case B the solution where $y \in [d, 1]$ is applied. In case C the solution for case B is still applicable for $y \in [b, 1]$ but now $\eta(b)$ and $u(b)$ become the depth and velocity at the lateral boundary of the ambient fluid. The general solutions are derived by first substituting the across-stream pressure (2.16) into the geostrophic equation (2.13). This expression is then differentiated and

https://doi.org/10.1017/S0022112004001351 Published online by Cambridge University Press

by applying (2.18) gives the general solution for the across-stream depth,

$$y \in [b, d]: \quad \eta(y) = \eta_0 \cosh Wy + u_0 \sinh Wy. \tag{2.19}$$

The associated general solution for the across-stream velocity is

$$y \in [b, d]: \quad u(y) = u_0 \cosh Wy + \eta_0 \sinh Wy. \tag{2.20}$$

Conservation of volume flux

The inward flux must equal the outward flux across the up- and downstream cross-sections. This is described by the following integral where the upstream discharge is simply c:

$$c = -\int_b^1 \int_0^{1-r} u_D(y)\,\mathrm{d}z\,\mathrm{d}y = -\int_b^1 u_D(y)(1-\eta)\,\mathrm{d}y \tag{2.21}$$

(see figure 4*a*). To integrate (2.21) the potential vorticity (2.18) and geostrophic relationship (2.13) are substituted, hence the terms are expressed as exact integrals:

$$c = \frac{1}{W}\left[\tfrac{1}{2}u_D^2 + p_D + Wcy\right]_b^1 \tag{2.22}$$

Conservation of momentum

The condition of conservation of momentum is satisfied by integrating the momentum equations (2.8) and (2.9) over the rectangular volume, V, connecting up- and downstream cross-sections (see figure 4*b*). In order to simplify the integral the divergence theorem is applied to the advective and pressure terms enabling them to be expressed as surface integrals. At rigid boundaries $\boldsymbol{u}\cdot\boldsymbol{n} = 0$:

$$\int_{A_U+A_D} \boldsymbol{u}(\boldsymbol{u}\cdot\boldsymbol{n})\,\mathrm{d}S + \int_{\partial V} p\boldsymbol{n}\,\mathrm{d}S = -\int_{V_a} W\boldsymbol{k}\times\boldsymbol{u}\,\mathrm{d}V - Wc\boldsymbol{j}\int_V \mathrm{d}V + \boldsymbol{k}\int_{V_c}\mathrm{d}V. \tag{2.23}$$

The j- and k-components of (2.23) merely express the balance between the pressure force, and Coriolis and buoyancy forces respectively. The i-component is the useful part of the equation,

$$\int_{A_U} \left(u_U^2 + p_U\right)\mathrm{d}A = \int_{A_a} \left(u_D^2 + p_D\right)\mathrm{d}A + \int_{A_c} p_c\,dA + W\int_{V_a} v\,\mathrm{d}V \tag{2.24}$$

where the surface A_D consists of A_c, the current, and A_a, the ambient fluid. The term on the left-hand side and the first term on the right-hand side of (2.24) are the momentum flux plus cross-sectional pressure acting on the ambient fluid up- and downstream respectively. The second term is the cross-sectional pressure acting on the current. In the third term, v is the across-stream component of the ambient fluid velocity, which induces a Coriolis force aimed upstream as the ambient fluid is accelerated around the current. This integral is equivalent to

$$W\int_{V_a} v\,\mathrm{d}V = W\int_0^1 Q_c(y)\,\mathrm{d}y \tag{2.25}$$

where $Q_c(y)$ is the volume flux at y across a vertical plane (see figure 4*c*). Hence $Q_c(y)$ can be evaluated knowing the flux in, cy, and out, $Q(0;y)$, of a region connecting up- to downstream, i.e.

$$Q_c(y) = cy - Q(0;y). \tag{2.26}$$

https://doi.org/10.1017/S0022112004001351 Published online by Cambridge University Press

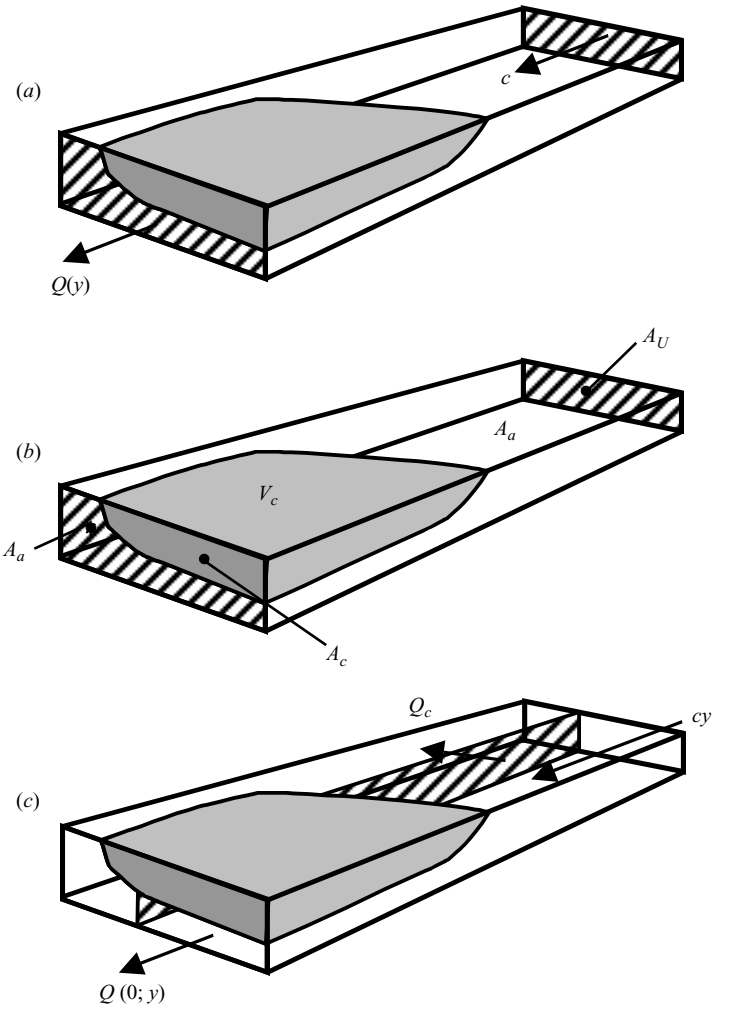


FIGURE 4. Sketches of integrals. (*a*) The cross-sectional area over which the downstream velocity is integrated. (*b*) The volume, V, bounded by ∂V, over which the momentum equation is integrated. The parts of V containing the ambient fluid and the current are V_a and V_c respectively. The up- and downstream faces of ∂V are A_u and A_D, where A_D is composed of A_c and A_a. (*c*) The fluxes into and out of a volume bounded by a vertical plane at y where the across-stream flux is Q_c. (Adapted from Hacker 1996).

The relation

$$Q(0;y) = \frac{1}{W}[B_D]_{y_0}^{y_1} \tag{2.27}$$

is substituted into (2.26) enabling the momentum integral (2.24) to be solved.

2.3. *Foundations of the rotating energy-dissipation theory*

The Bernoulli equation for rotating flow has the form

$$B = \tfrac{1}{2}|\boldsymbol{u}|^2 + p + Wcy = \text{constant along streamlines.} \tag{2.28}$$

The third term on the right-hand side is the potential energy a fluid element possesses due to its position in the potential field of the body force of translation. This is equivalent to the gravitational potential energy in the non-rotating Bernoulli equation.

https://doi.org/10.1017/S0022112004001351 Published online by Cambridge University Press

As the fluid element moves across-stream work must be done against the body force of translation, therefore it gains potential energy. In order for the total energy to remain constant the fluid element must move into a region of lower pressure or decelerate.

In the rotating problem the dissipation of energy will be accompanied by the loss of potential vorticity. In considering the limitations of his work Hacker (1996) derives an expression coupling the energy $\Delta e(y)$ and potential vorticity $\Delta q(y)$ lost in moving across-stream to the position y. He introduces $\Delta e(y)$ into the Bernoulli equation (2.3.1) to give

$$WcY = \tfrac{1}{2}u_D^2 + P_D + Wcy + \Delta e(y), \tag{2.29a}$$

and $\Delta q(y)$ into the shallow-water potential vorticity equation resulting in

$$\frac{\mathrm{d}u_D}{\mathrm{d}y} + W(1-\eta)\Delta q(y) = W\eta. \tag{2.29b}$$

Continuity of volume flux (2.21) between the positions b and y yields

$$cY(y) = -\int_b^y u_D(y)(1-\eta(y))\,\mathrm{d}y. \tag{2.30}$$

Substituting (2.29a, b) and (2.13) into (2.30) gives

$$\Delta e(y) - \Delta e(b) = W\int_b^y u_D(s)\Delta q(s)(1-\eta(s))\,\mathrm{d}s \tag{2.31}$$

which shows that if there is variation in energy loss across-stream then there will be an associated pertubation in the potential vorticity flux. Hacker identified the difficulties in solving (2.31) due to insufficient information. However as a first step he suggests examining the case of

$$\Delta e(y) = \text{constant},$$

where according to (2.31)

$$\Delta q(y) = 0.$$

Thus assuming uniform energy loss implies conservation of potential vorticity and is thus a greatly simplifying assumption. This assumption is utilized in the next section, where the solution to the rotating energy loss theory is presented.

3. Solution for rotating gravity currents with energy dissipation

The approach taken to include dissipation in the present study is based on the method used by Benjamin for the non-rotating case. First a head loss term is introduced into the Bernoulli equation and the assumption of uniform energy loss across the stream is made. Next a solution for the propagation rate of the interface, c, is obtained using the continuity equation. The momentum integral is solved by using the volume flux, $Q(0;y)$. For each case the momentum equation is expressed in terms of one of the principle variables, with W and η_0 retained as pre-set constants, and solved numerically using the Newton–Raphson method.

Introduction of the head loss term

To identify the energy loss a head loss term is introduced into the Bernoulli equation (2.28) and applied at the right-hand boundary of the ambient fluid to give

$$B_D(b) = \tfrac{1}{2}u_D^2 + p_D + Wcb + \Delta e(b). \tag{3.1}$$

https://doi.org/10.1017/S0022112004001351 Published online by Cambridge University Press

It is assumed that the energy loss is uniform across the stream, therefore

$$\Delta e(b) = \Delta E = \text{constant}.$$

Obtaining an expression for ΔE requires some detailed manipulations which are given in the Appendix, eventually giving

$$\Delta E = \frac{1}{2(1-b)}\left\{\frac{1}{W}\left[-\frac{2}{3}u_D^3 + \eta u_D\right]_b^d + U_D^2(1-d) - b - c^2\right\}. \tag{3.2}$$

Continuity of volume flux

Continuity of volume flux is described by the integral (2.21). To integrate (2.21) the potential vorticity equation (2.18) and the geostrophic equation (2.13) are used, enabling (2.21) to be expressed in terms of exact differentials, hence

$$\begin{aligned} c &= -\int_b^1 u_D(y)(1-\eta(y))\,\mathrm{d}y \\ &= \frac{1}{W}\left(\int_b^d + \int_d^1\right)\left(\frac{\mathrm{d}p_D}{\mathrm{d}y} + Wc + u_D\frac{\mathrm{d}u_D}{\mathrm{d}y}\right)\mathrm{d}y \\ &= \frac{1}{W}\left[p_D + Wcy + \tfrac{1}{2}u_D^2\right]_b^d + \frac{1}{W}\left[p_D + Wcy + \tfrac{1}{2}u_D^2\right]_d^1. \end{aligned}$$

Substituting for the downstream pressure fields, (2.16) and (2.17), yields

$$c = \frac{1}{W}\left[\tfrac{1}{2}u_D^2(1) - \eta(d) - WU_D(1-d) + \eta(b) - \tfrac{1}{2}u_D^2(b)\right]. \tag{3.3}$$

Conservation of momentum

Solving the momentum integral (2.24) again requires some detailed manipulations, given in the Appendix. The final result is an expression for c^2,

$$c^2 = \frac{1}{W}\left[\tfrac{2}{3}u_D^3 - \eta u_D\right]_b^d + U_D^2(1-d) - b + 2(1-b)\left\{\tfrac{1}{2}u_D^2(b) - \eta(b)\right\}. \tag{3.4}$$

Solving the equations

To summarize, the governing equations are equations (3.2), (3.3) and (3.4), which are equations for energy, volume and momentum respectively. It is worth noting that the last two of these contain expressions of the form $(\eta(b) - \frac{1}{2}u_D^2(b))$, which are zero in the energy-conserving theory. Thus the corresponding equations in Hacker's energy-conserving theory are similar to (3.3) and (3.4) but without the last terms. In the Appendix we also show that the equations given here tend to the non-rotating equations of § 2.1 as W tends to zero.

The governing equations are defined in terms of $\eta(y)$, $u_D(y)$, c, b and d, which in turn can all be expressed as functions of u_0 and the pre-set constants W and η_0, using the flow structure equations (2.19) and (2.20) for each of the three flow geometries (cases A, B and C). Thus, for given values of W and η_0, we are effectively solving for u_0. The detailed equations and solution methods for each of the three cases are given in the Appendix, together with the transition points between the cases. The detailed results are given in the next section.

https://doi.org/10.1017/S0022112004001351 Published online by Cambridge University Press

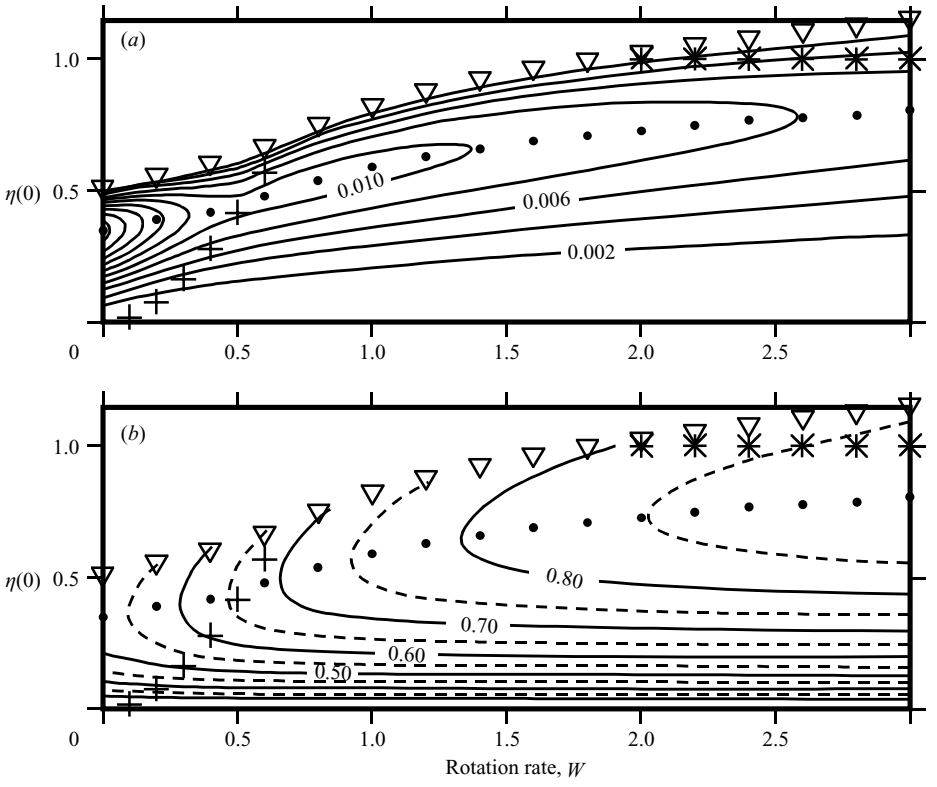


FIGURE 5. Contour plots of the solutions for the energy loss ΔE and front speed c, as the rotation rate, W and the fractional depth are varied. ▽, dissipationless solution (Hacker); +, transition between case A and B; ✳, transition between case B and C; ●, maximum value. (*a*) Energy loss ΔE solutions – if the upstream volume flux is restricted, then the energy-conserving flow will not be possible. The volume flux and hence the level of dissipation are set by the fractional depth of the current. As the level of the rotation is increased for a particular fractional depth, the energy loss decreases. For shallow currents ($\eta(0) \to 0$) the energy loss is zero (a result consistent with that obtained by Benjamin for non-rotating gravity currents). (*b*) Front speed c solutions – the maximum front speed coincides with the maximum energy loss, ΔE. Generally the front speed increases with rotation rate. However, at shallow depths the front speed becomes constant irrespective of the rotation rate.

4. Results and discussion

Main results

In the energy loss theory the principle variables are a function of two parameters, i.e. η_0 and W. To illustrate the solutions the results are plotted on contour graphs. The method used to contour the results is Delaunay Triangulation and the data set consists of more than 3000 data points. Figures 5(*a*) and 5(*b*) show the solutions for ΔE (3.2) and c (3.3).

These two variables show similar behaviour. As η_0 is decreased from the energy-conserving value at a particular level of rotation, ΔE and c increase until they reach a maximum value. The maxima for ΔE and c both occur in the same position (W, η_0). However, for ΔE the values of the maxima generally decrease with increasing rotation, whilst for c the values increase. For each level of rotation within a certain range two depths are possible for a particular value of ΔE and c. For shallow depths,

https://doi.org/10.1017/S0022112004001351 Published online by Cambridge University Press

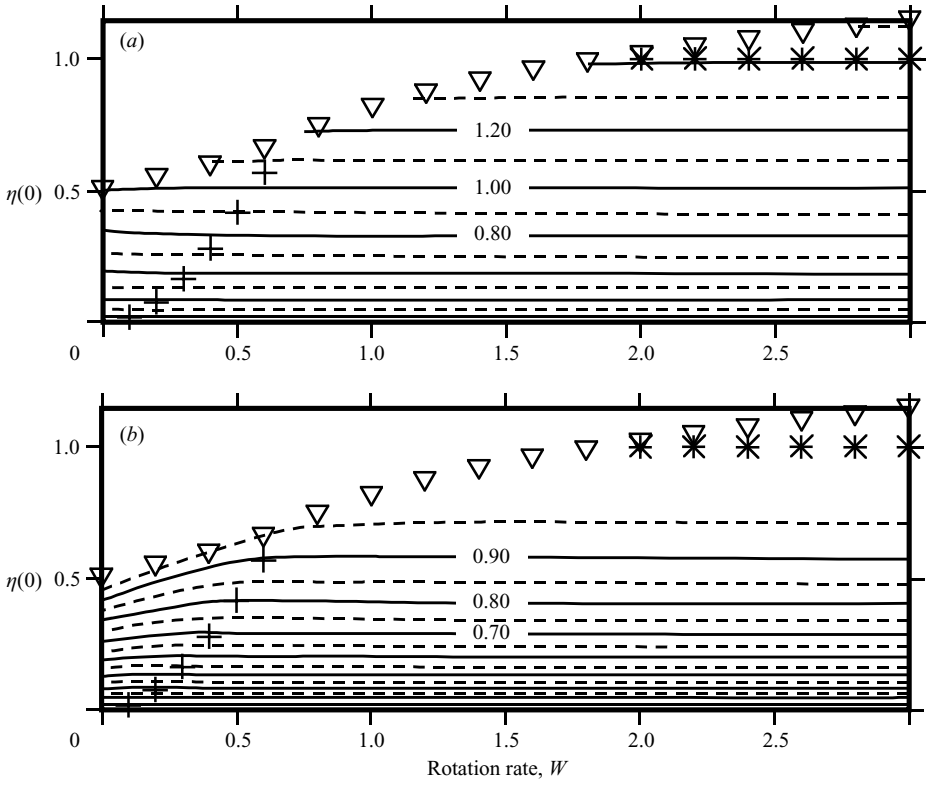


FIGURE 6. Contour plots of the solutions for the ambient fluid velocities (always negative) at the right-hand wall, u_0 and at $y = d$, $u_D(d)$, as the rotation rate, W, and the fractional depth, $\eta(0)$ are varied. (See figure 5 for an explanation of the symbols used.) (a) Ambient fluid speed at the right-hand wall, $-u_0$ – the velocity u_0 is dependent on the fractional depth of the current. The level of rotation has a minimal effect. (b) Ambient fluid speed at $y = d$, $-u_D(d)$ – for low rotation rates (case A) the velocity $u_D(d)$ increases with rotation for a particular fractional depth. At higher rotation rates the velocity is dependent on the fractional depth only.

c becomes relatively constant and rotation has little effect. It is interesting to note that the energy loss tends to zero for shallow currents at all levels of rotation. Figures 6(a) and 6(b), show the solutions for the ambient fluid velocity (2.20) at the boundaries $y = 0$ and $y = d$, i.e. u_0 and $u_D(d)$ respectively.

In case A, where the current fills the full width of the channel, as the rotation rate increases for a particular depth, η_0, the magnitude of the velocity at the right-hand wall, u_0, decreases minimally from the non-rotating solution, whilst at the left-hand wall the speed, $|u_D(1)|$, increases. However, at very shallow depths rotation has no discernible effect on either of the velocities. What is striking is that once the current has departed from the left-hand wall the strength of rotation becomes ineffectual and consequently the velocity is primarily dependent on the depth, η_0. The velocity, $u_D(b)$, for the dissipationless case equals $-\sqrt{2}$, and as the depth of the current is reduced this velocity decreases until the current no longer outcrops on the bottom boundary. The transition from $u_D(b)$ to u_0 at $\eta_0 = 1$ occurs smoothly. Figures 7(a) and 7(b) illustrate the solutions for the widths b and d. In case C, b decreases from the dissipationless solution. For shallow currents the onset of case B, where the current outcrops on the

https://doi.org/10.1017/S0022112004001351 Published online by Cambridge University Press

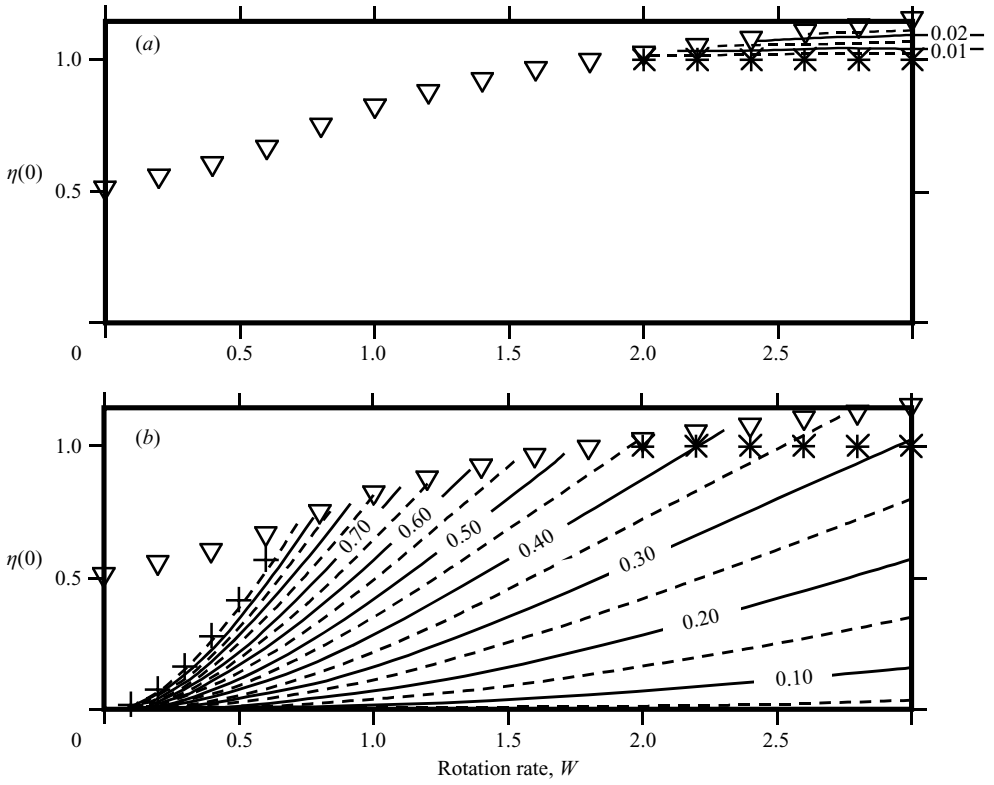


FIGURE 7. Contour plots of the solutions for the current width at the bottom boundary, b (case C only) and the free surface d, as the rotation rate, W, and the fractional depth, $\eta(0)$ are varied. (See figure 5 for an explanation of the symbols used.) (a) Current width at the bottom boundary, b – in case C, b is seen to decrease from Hacker's dissipationless solution to zero at $\eta(0) = 1$, i.e. the transition from case B to C. (b) Current width at the free surface, d – the transition to case B occurs at much lower levels of rotation for shallower currents with energy loss.

surface ($y = d$), occurs at much lower levels of rotation than in the energy-conserving case. As W increases the ratio of d/η_0 decreases as expected.

Pressure and momentum

To investigate the effect of reducing the current depth on the ambient fluid across the stream, three-dimensional graphs are presented. Note that η_0 is varied rather than W. The surfaces in figures 8(a) and 8(b) are the pressure, $p(y)$ beneath the current (2.16) and in the free-stream (2.17), and velocity, $u_D(y)$ (2.20), respectively, for $W = 3.0$.

The equations governing the structure of the flow in the energy-conserving case are still applicable. Therefore the pressure is a result of the hydrostatic and geostrophic pressure gradients. At the right-hand wall ($y = 0$) as η_0 is decreased the pressure increases. This is associated with a reduction in the velocity. In the energy-conserving case the geostrophic pressure gradient causes the pressure to increase across the stream. As the depth is decreased the difference in pressure from widths b to d lessens, until the pressure becomes relatively constant across the stream. Hence the hydrostatic and geostrophic pressure gradients become almost equal and the shear in the free stream around the current becomes insignificant. For the current the pressure is also constant across the stream according to (2.14). Although the pressure

https://doi.org/10.1017/S0022112004001351 Published online by Cambridge University Press

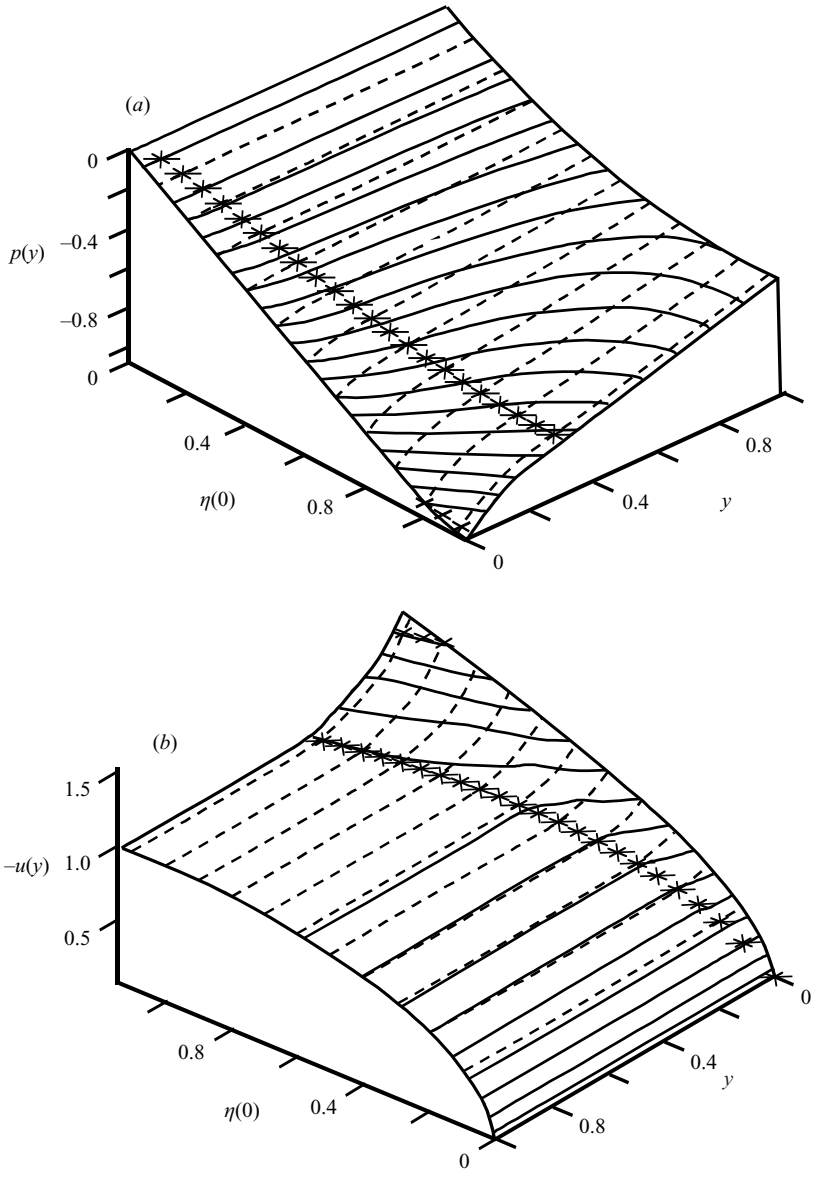


FIGURE 8. Surface plots to illustrate the across-stream variation in pressure, $p(y)$, and velocity, $u_D(d)$, for the ambient fluid where $W = 3.0$. At $W = 3.0$ the current has departed from the left-hand wall ($y = 1$) and outcrops at $y = d$ on the free surface. For the energy-conserving depth the current fills the full depth of the channel, outcropping on the bottom boundary at $y = b$. $*$, $y = d$, current outcrops on the free surface (transition from case B to C); $+$, $y = b$, current outcrops on the bottom boundary (transition from case B to C). (*a*) Across-stream pressure, $p(y)$ – for the energy-conserving depth the pressure increases across the stream with the greatest pressure gradient beneath the current. As the fractional depth is decreased ($\eta(0) \to 0$), the across-stream pressure increases, particularly at the right-hand wall ($y = 0$). At shallow depths the pressure is constant. (*b*) Across stream velocity, $u_D(y)$ – for the energy-conserving depth there is a strong shear beneath the current. As the fractional depth is reduced ($\eta(0) \to 0$) the speed is seen to decrease at the right-hand wall from $u_D(b) = -2^{1/2}$, tending to zero for shallow currents. In the free stream ($d \leqslant y \leqslant 1$) the velocity is constant and decreases for shallow currents.

https://doi.org/10.1017/S0022112004001351 Published online by Cambridge University Press

difference across the stream is minimal for shallow currents, if the ambient fluid is to be accelerated from up- to downstream there must be a positive net momentum flux between up- and downstream cross-sections, i.e. the pressure forces acting upstream must be greater than those due to buoyancy and the Coriolis forces acting downstream.

To consider this further the net momentum flux for the ambient fluid is calculated as η_0 and W are varied. The net momentum flux, M, i.e. the net force acting on the control volume is derived from (2.24) to give the same expression as in the energy-conserving case where

$$M = \int_{A_a} (u_D^2)\,\mathrm{d}A - \int_{A_u} (c^2)\,\mathrm{d}A. \tag{4.1}$$

The labels A_a and A_u refer to the ambient fluid downstream and upstream respectively. By substituting (2.18) and (2.20) and using the hyperbolic identity for cosh $2x$ the integral (4.1) is solved for each of the cases A, B and C. Figure 9(a) shows the net momentum flux in the ambient fluid. For the energy-conserving case the momentum flux decreases with increasing rotation. This trend is also apparent when η_0 is held constant at a value less the dissipationless depth and the level of rotation is increased. However, M is more sensitive to a reduction in η_0. Initially M decreases nearly linearly until at shallower depths the decrease slows as M tends to zero. This implies that the forces acting downstream on the ambient fluid cross-section diminish considerably with decreasing η_0. Therefore, one would expect the mean velocity across the ambient cross-section to show a significant reduction as η_0 decreases. The mean velocity is as defined in Hacker's dissipationless theory, since the flow structure equations are unaltered by the loss of energy for this simple case, where

$$\overline{u}_D = \frac{\displaystyle\int_{Aa} u_D(y)\,\mathrm{d}A}{\displaystyle\int_{Aa} \mathrm{d}A} = \frac{-c}{\displaystyle\int_b^1 (1-\eta(y))\,\mathrm{d}y}. \tag{4.2}$$

The integral in (4.2) is evaluated by substituting the exact differential (2.18). Hence the general solution is obtained, which is solved for each flow geometry. The results are plotted in figure 9(b). As expected the mean speed, $\bar{q}_D = |\bar{u}_D| = -\bar{u}_D$, decreases as the current becomes shallower. However there is not a decrease in $\bar{q}_D$ corresponding to the reduction in M as the level of rotation is increased. In fact $\bar{q}_D$ remains relatively constant for case B where $\eta_0 < 0.5$. As the level of rotation increases the cross-sectional area of the ambient fluid must also increase. To quantify the change in the cross-sectional area downstream in the ambient fluid, A_D, the following integral is evaluated:

$$A_D = \int_{A_a} \mathrm{d}A = \int_b^1 (1-\eta(y))\,\mathrm{d}y. \tag{4.3}$$

The solutions for A_D are plotted in figure 9(c). As W increases A_D increases in a similar manner to the decrease in the momentum flux.

These theoretical results can be explained simply using a similar argument to that proposed by Hacker in his explanation for the increase in c with W. In the energy-conserving case with simple flow, as W increases it causes A_D to become greater, however $\bar{q}_D$ remains relatively constant. Therefore, the downstream volume flux will increase. Hacker reasoned that the greater volume flux downstream would by continuity require an increase in the speed of the oncoming flow c. In the energy loss case in figure 5(b) one can see that when η_0 is large c increases as the level of rotation

https://doi.org/10.1017/S0022112004001351 Published online by Cambridge University Press

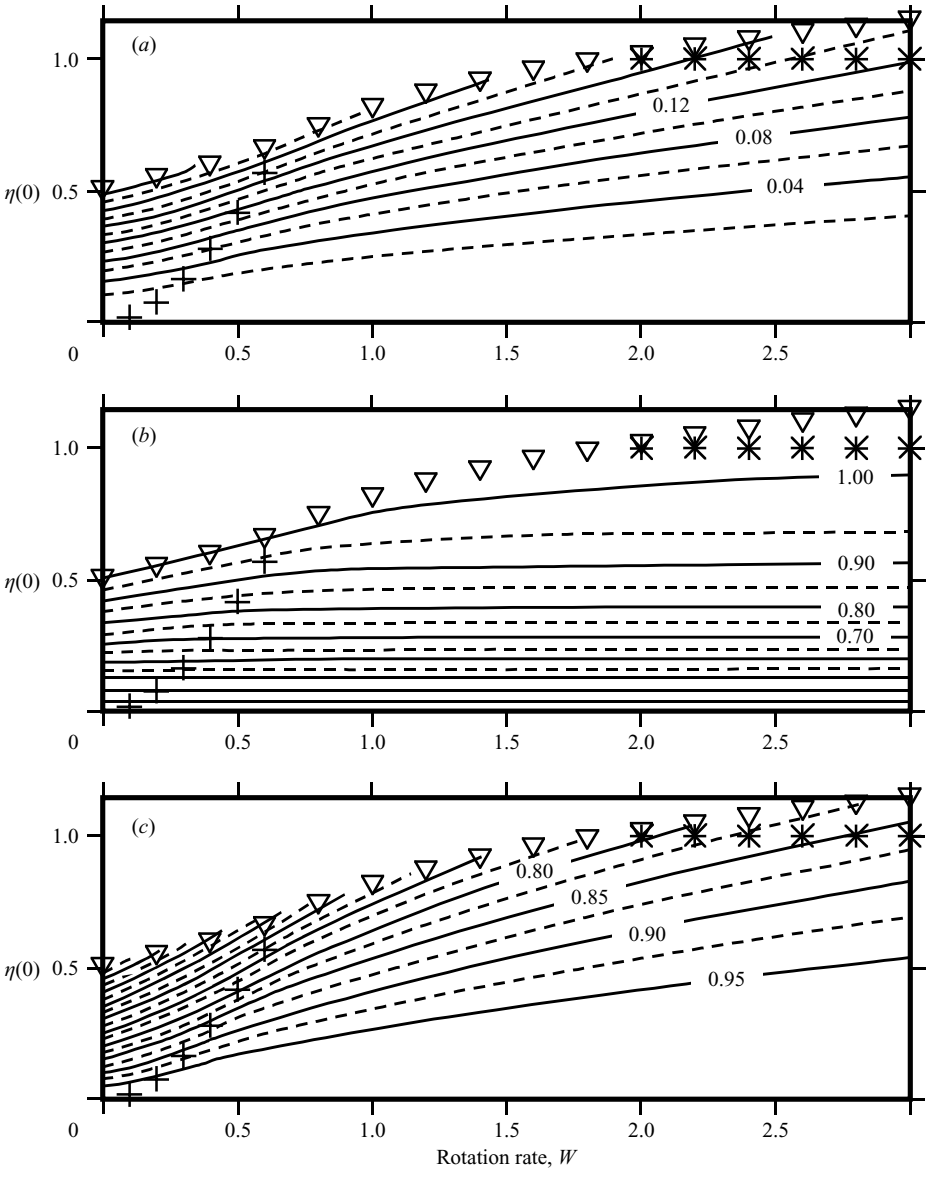


FIGURE 9. Contour plots of the solutions for (*a*) net momentum flux M, (*b*) mean speed $\bar{q}_D$ and (*c*) cross-sectional area A_D for the ambient fluid, as the rotation rate W and fractional depth $\eta(0)$ are varied. (See figure 5 for an explanation of the symbols used.)

rises; however at shallow depths c becomes relatively constant. From figure 9(*a*) it is observed that at shallow depths as W is increased M remains close to zero. Therefore increasing W at shallow depths no longer causes a marked acceleration of the ambient fluid as it reaches the downstream cross-section. The cross-sectional area, A_D, is tending to 1 and hence $\bar{q}_D$ tends to c. The effect on c of lowering the depth, η_0, for a constant value of W is that initially c increases until it reaches a maximum value which coincides with the maximum energy loss (figure 5*b*). Further reduction of η_0 causes c to decrease. Therefore the initial response to a reduction in η_0 is that the downstream volume flux in the ambient fluid must increase, in order to accommodate the increased

https://doi.org/10.1017/S0022112004001351 Published online by Cambridge University Press

speed of the upstream flow. In the range of depths greater than that at the maximum value of c this is indeed the case. The cross-sectional area increases, whilst the decrease in $\bar{q}_D$ is only slight. Below the maximum A_D continues to increase, whilst the decrease in $\bar{q}_D$ now becomes significant. Therefore, there is a reduction in the volume flux downstream requiring c to decrease. This argument is based on the assumption that the velocity is uniform across the stream. Although this is not the case close to the energy-conserving solutions, at shallow depths the velocity is indeed constant across the channel, as shown in figure 8(b). Therefore this simple argument based on continuity does give an explanation for the variation of c as η_0 and W are varied.

Energy

Earlier the method used to include energy loss in the non-rotating theory of Benjamin (1968) was discussed. The non-rotating solutions have been included at $W = 0$ in the contour graphs of figures 5 to 9. However, to provide a clearer comparison with the non-rotating solutions for the variables Q(2.6), c (2.5), and ΔE(2.4), two-dimensional graphs are plotted for $0 \leqslant W \leqslant 3$ in figure 10. The endpoints on the right-hand side of each curve represent the energy-conserving solutions. The trends identified for the non-rotating case are again apparent. In figure 10(a), the energy loss, ΔE (3.2), is found to equal zero at the energy-conserving solution and as η_0 tends to zero for all values of W. The magnitude of the maximum value of ΔE initially decreases significantly as the level of rotation increases for case A. At $W \sim 0.5$ there is a slight increase in ΔE; thereafter it continues to decrease at a reduced rate. In figure 10(b), the front speed, c (3.4), exhibits the characteristic curve identified by Benjamin in the non-rotating case, where c corresponds to two values of η_0 within a certain range. The maximum values for c coincide with the maxima for ΔE. As W increases c also increases; however at shallow depths c becomes relatively constant for all values of W. Note that c is equivalent to the downstream volume flux of the ambient fluid from equation (2.21). The volume flux of the current, Q, is shown in figure 10(c). As in the non-rotating case the maximum discharge of the current occurs at the energy-conserving depth. Q decreases as the current becomes shallower and the level of rotation is increased, as one would expect.

Benjamin explained the two alternative depths for c by referring to the hydraulic equations of Lamb (1932). At the dissipationless depth the downstream ambient flow is supercritical according to (2.5). By allowing for dissipation Benjamin suggests that the ambient flow would adjust to a deeper depth through a mechanism such as a hydraulic jump. Hence, the flow would become subcritical. The similar behaviour of c for the rotating case implies that the ambient fluid would adjust to a deeper depth, resulting in a shallower current. Benjamin also calculates a Froude number based on the propagation rate of the cavity, c. For shallow currents the Froude number $(c/(g(H-h))^{1/2}$ tends to $\sqrt{2}$. The results of the theoretical study so far have shown that for shallow currents the level of rotation has little effect on c. Therefore, one might predict that the Froude number would tend to $\sqrt{2}$ as for non-rotating gravity currents: figure 11 shows that this is indeed the case.

5. Conclusions

We have developed a comprehensive theory to describe the flow of a gravity current in a rotating rectangular channel of arbitrary depth and width. This is a substantial advance on previous work, which had significant limitations on the range of applicability of their solutions. The approach used is in the same spirit

https://doi.org/10.1017/S0022112004001351 Published online by Cambridge University Press

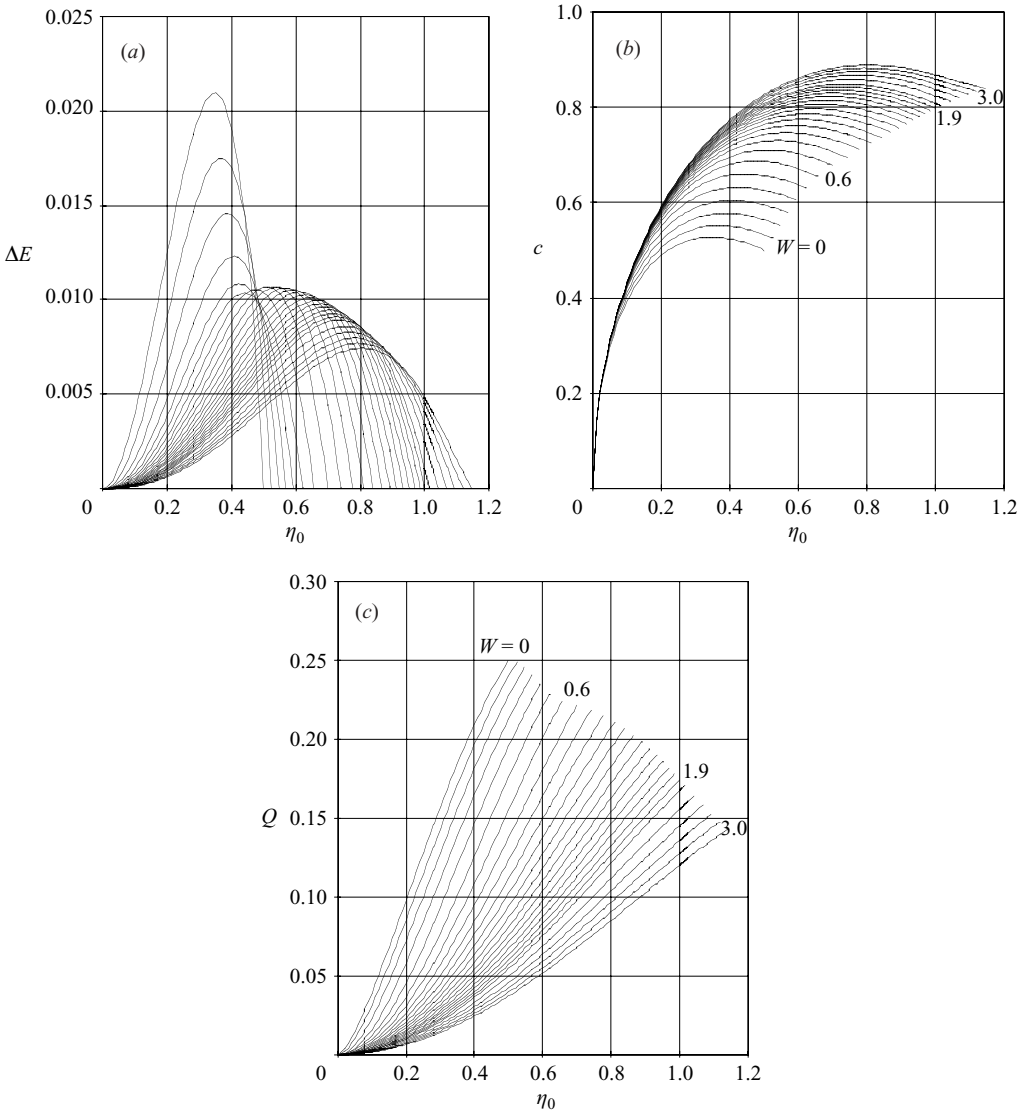


FIGURE 10. Plots of energy loss ΔE, front speed c and discharge Q versus fractional depth η_0. The same set of values of W are used in all three plots, with an interval of 0.1 from 0 to 2.0 and an interval of 0.2 from 2.0 to 3.0. (*a*) Energy loss ΔE – as the fractional depth is decreased below the dissipationless value there is a positive loss of energy. (*b*) Front speed c – in agreement with the non-rotating energy loss theory (Benjamin 1968) two values of η_0 correspond to c within a certain range. The maximum value of c also coincides with the maximum energy loss, ΔE. (*c*) In agreement with the non-rotating energy loss theory (Benjamin 1968) the maximum discharge occurs at the energy-conserving depth.

as the approach used by Benjamin (1968) to incorporate energy dissipation in non-rotating gravity currents, and effectively fills in the parameter space that lies between Benjamin's non-rotating results and the energy-conserving rotating theory of Hacker (1996), matching those theories in the appropriate limits.

As the effect of rotation increases, three different types of flow (and the transitions between them) have been identified and quantified. In case A (weakly rotating) the

https://doi.org/10.1017/S0022112004001351 Published online by Cambridge University Press

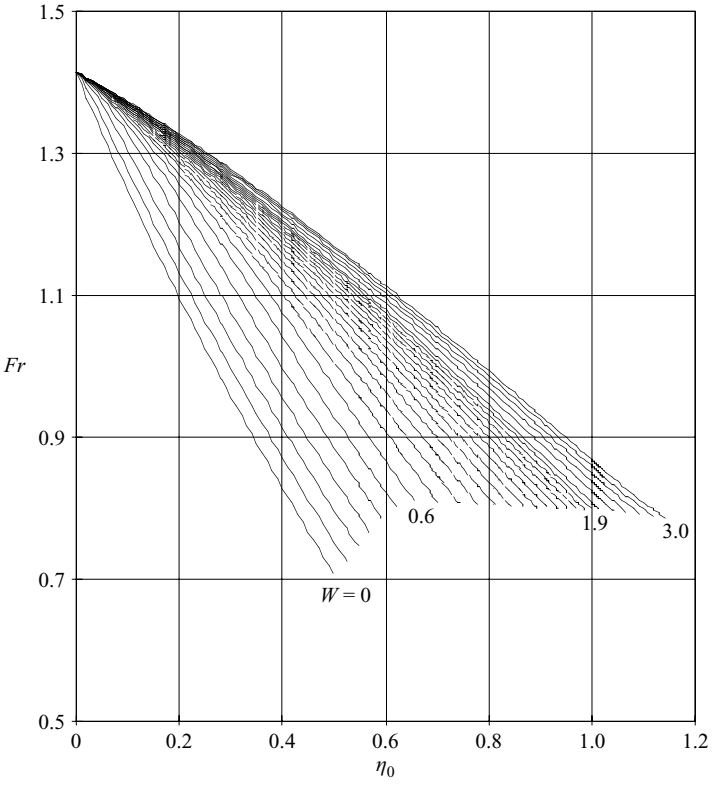


FIGURE 11. Froude number Fr versus fractional depth η_0. In agreement with the non-rotating energy loss theory (Benjamin 1968) the Froude number tends to $\sqrt{2}$ as η_0 tends to zero.

flow occupies the full width of the channel, but with a sloping interface. In case B (intermediate rotation) the current occupies only part of the width (and part of the depth) of the channel. For strong rotation (case C) the interface slope is sufficiently large that it outcrops on the top and bottom of the channel. The main features can be understood in terms of continuity and energy, in a similar fashion to non-rotating gravity currents. Trends common to both the rotating and non-rotating energy dissipation theories include

(i) maximum energy loss coincides with the maximum values for the front speed;
(ii) maximum volume flux of the current occurs at the energy-conserving depth;
(iii) two alternative depths are possible for each value of c within a certain range;
(iv) Froude number tends to $\sqrt{2}$ for shallow currents.

The two alternative depths for a certain value of front speed were attributed by Benjamin to the adjustment from supercritical flow at the dissipationless depth to subcritical flow as energy is lost though a mechanism such as a hydraulic jump. In addition to these trends the rotating energy loss theory predicts that the maximum energy loss will decrease with increasing rotation and associated with this will be an increase in the maximum front speed. For shallow currents the front speed will remain constant. The velocity in the ambient fluid appears to be primarily dependent on the fractional depth, with the rotation rate only exerting a slight influence in case A. The ambient fluid velocity is at its maximum at the energy-conserving depth, decreasing as η_0 tends to zero. The theory predicts that the width of the current is dependent

https://doi.org/10.1017/S0022112004001351 Published online by Cambridge University Press

on both the fractional depth and the rotation rate, with the width decreasing as the rotation rate increases.

The theory we have presented here assumes that there is no shear in the gravity current. In Part 2 (Martin *et al.* 2004) we will relax this condition and instead assume a given upstream potential vorticity boundary condition. This allows for flows in which the velocity varies across the width of the gravity current.

Much of this work was carried out at the School of Ocean and Earth Science, University of Southampton, where J. R. M. was supported by a PhD studentship from the Natural Environment Research Council (UK) and G. F. L. S. was supported by a University Research Fellowship from the Royal Society, London. J. R. M. was granted sabbatical leave to prepare this paper by Southampton University Hospitals NHS Trust. The authors would like to thank Dr David Smeed and Professor Steve Thorpe for useful discussions and advice.

Appendix. Detailed derivation and solution of the governing equations

A.1. *Derivations*

In this section some of the detailed derivations of the main equations are given.

A.1.1. *Energy dissipation*

To obtain a solution for ΔE we make use of the momentum integral (2.24) as follows. The first of the unknown parameters, p_0, is obtained by applying the Bernoulli equation to a streamline along the right-hand wall, joining the foremost stagnation point (0, 0, 1) to the upstream flow, hence

$$p_0 = -\tfrac{1}{2}c^2. \tag{A 1}$$

The upstream integral is evaluated using (2.15), (A 1) and recalling that $u_u = c$, so that (2.24) becomes

$$\tfrac{1}{2}c^2 = \int_{A_a} \left(u_D^2 + p_D\right) \mathrm{d}A + \int_{A_c} p_c \,\mathrm{d}A + W \int_{V_a} v \,\mathrm{d}V. \tag{A 2}$$

Integrating the first integral with respect to z gives

$$\int_{A_a} \left(u_D^2 + p_D\right) \mathrm{d}A = \int_b^1 \left(u_D^2 + p_D\right)(1-\eta)\,\mathrm{d}y. \tag{A 3}$$

To solve (A 3) the following substitution is required. Conservation of volume flux (2.21) between y_0 and y gives

$$Q_D(y_0; y) = -\int u_D(y)(1-\eta(y))\,\mathrm{d}y$$

which, according to (2.22) and (2.27) becomes

$$Q_D(y_0; y) = \frac{1}{W}\left[\tfrac{1}{2}u_D^2 + p_D + Wcy\right]_{y_0}^{y} = \frac{1}{W}[B_D]_{y_0}^{y}; \tag{A 4}$$

therefore

$$\left(\tfrac{1}{2}u_D^2 + p_D\right)\Big|_y = B_D(y) - B_D(y_0) + \left(\tfrac{1}{2}u_D^2 + p_D\right)\Big|_{y_0} - Wcy|_y + Wcy|_{y_0}. \tag{A 5}$$

https://doi.org/10.1017/S0022112004001351 Published online by Cambridge University Press

Substituting (A 5) into (A 3) gives

$$\int_b^1 \left(u_D^2 + p_D\right)(1-\eta)\,\mathrm{d}y = \int_b^1 \left(B_D(y) - Wcy + \tfrac{1}{2}u_D^2 - \eta\left(u_D^2 + p_D\right)\right)\mathrm{d}y + (1-b)\left\{-B_D(b) + Wcb + \tfrac{1}{2}u_D^2(b) + p_D(b)\right\}. \quad (A\,6)$$

The third integral in (A 2) is simplified by substituting (2.26) into (2.25) and noting that $Q_D(0, y) = 0$ when $y \in [0, b]$ gives

$$W\int_{V_a} v\,\mathrm{d}V = W\int_0^b cy\,\mathrm{d}y + W\int_b^1 (cy - Q_D(y))\,\mathrm{d}y.$$

Using (2.27) the above equation becomes

$$W\int_{V_a} v\,\mathrm{d}V = \tfrac{1}{2}Wcb^2 + \int_b^1 (Wcy - B_D(y))\,\mathrm{d}y. \quad (A\,7)$$

Substituting (A 6) and (A 7) into the momentum integral (A 2) gives

$$\tfrac{1}{2}c^2 = \int_b^1 \left(\tfrac{1}{2}u_D^2 - \eta\left(u_D^2 + p_D\right)\right)\mathrm{d}y + (1-b)\left\{-B_D(b) + Wcb + \tfrac{1}{2}u_D^2(b) + p_D(b)\right\} + \int_{A_c} p_c\,\mathrm{d}A + \tfrac{1}{2}Wcb^2 \quad (A\,8)$$

The pressure fields (2.16) and (2.17) are substituted into the first integral in (A 8), noting that $\eta = 0$ for $y \in [d, 1]$:

$$\int_b^1 \left(\tfrac{1}{2}u_D^2 - \eta\left(u_D^2 + p_D\right)\right)\mathrm{d}y = \int_b^d \left(\tfrac{1}{2}u_D^2 - \eta u_D^2 + \eta^2 + \eta Wcy\right)\mathrm{d}y + \tfrac{1}{2}U_D^2(1-d). \quad (A\,9)$$

The pressure field for the current (2.14) is substituted into the second integral in (A 8), noting that $\eta = 1$ for $y \in [0, b]$:

$$\int_{A_c} p_c\,\mathrm{d}A = -\tfrac{1}{2}b - \tfrac{1}{2}Wcb^2 + \int_b^d \left(-\tfrac{1}{2}\eta^2 - Wcy\eta\right)\mathrm{d}y. \quad (A\,10)$$

When (A 9) and (A 10) are substituted into (A 8) the momentum integral becomes

$$\tfrac{1}{2}c^2 = \int_b^d \left(\tfrac{1}{2}u_D^2 - \eta u_D^2 + \tfrac{1}{2}\eta^2\right)\mathrm{d}y + \tfrac{1}{2}U_D^2(1-d) - \tfrac{1}{2}b + (1-b)\left\{-B_D(b) + Wcb + \tfrac{1}{2}u_D^2(b) + p_D(b)\right\}. \quad (A\,11)$$

The head loss term is introduced into (A 11) through the Bernoulli function, hence (A 11) becomes

$$\tfrac{1}{2}c^2 = \int_b^d \left(\tfrac{1}{2}u_D^2 - \eta u_D^2 + \tfrac{1}{2}\eta^2\right)\mathrm{d}y + \tfrac{1}{2}U_D^2(1-d) - \tfrac{1}{2}b + (1-b)(-\Delta E). \quad (A\,12)$$

Making use of the potential vorticity equation (2.18), the geostrophic equation (2.13) and the across-stream ambient pressure (2.16) enables (A 12) to be expressed in terms of exact differentials. It is then easily integrated to give

$$c^2 = \frac{1}{W}\left[-\tfrac{2}{3}u_D^3 + \eta u_D\right]_b^d + U_D^2(1-d) - b + 2(1-b)(-\Delta E). \quad (A\,13)$$

https://doi.org/10.1017/S0022112004001351 Published online by Cambridge University Press

Rearranging (A 13) gives the governing energy loss equation with

$$\Delta E = \frac{1}{2(1-b)}\left\{\frac{1}{W}\left[-\tfrac{2}{3}u_D^3 + \eta u_D\right]_b^d + U_D^2(1-d) - b - c^2\right\}. \tag{A 14}$$

This is given as equation (3.2) in the main text.

A.1.2. *Conservation of momentum*

To solve the momentum integral we make use of expressions for the discharge, Q_D. Substitution is once again required for the first integral (A 3) in the momentum equation (A 2). According to (A 4)

$$W[Q_D]_{y_0}^{y} = \left[\tfrac{1}{2}u_D^2 + p_D + Wcy\right]_{y_0}^{y}; \tag{A 15}$$

therefore

$$\left(\tfrac{1}{2}u_D^2 + p_D\right)\Big|_y = W(Q_D(y) - Q_D(y_0)) + \left(\tfrac{1}{2}u_D^2 + p_D\right)\Big|_{y0} - Wcy|_y + Wcy|_{y0}. \tag{A 16}$$

Substituting (A 16) into (A 3) gives

$$\int_b^1 \left(u_D^2 + p_D\right)(1-\eta)\,\mathrm{d}y = \int_b^1 \left(W(Q_D(y) - cy) + \tfrac{1}{2}u_D^2 - \eta\left(u_D^2 + p_D\right)\right)\mathrm{d}y + (1-b)\left\{W(-Q_D(b) + cb) + \tfrac{1}{2}u_D^2(b) + p_D(b)\right\}. \tag{A 17}$$

The expression derived previously for the cross-stream velocity volume integral (A 7) and (A 17) are substituted into the momentum integral (A 2) which becomes

$$\tfrac{1}{2}c^2 = \int_b^1 \tfrac{1}{2}u_D^2 - \eta\left(u_D^2 + p_D\right)\mathrm{d}y + (1-b)\left\{W(-Q_D(b) + cb) + \tfrac{1}{2}u_D^2(b) + p_D(b)\right\} + \int_{Ac} p_c\,\mathrm{d}A + \tfrac{1}{2}Wcb^2. \tag{A 18}$$

The pressure fields (2.16) and (2.17) are substituted into the first integral in (A 18) to give (A 9) and the across stream pressure for the current (2.14) is substituted into the second integral to give (A 10), as in § A1.1. These are then substituted into (A 18) which becomes

$$\tfrac{1}{2}c^2 = \int_b^d \tfrac{1}{2}u_D^2 - \eta u_D^2 + \tfrac{1}{2}\eta^2\,\mathrm{d}y + \tfrac{1}{2}U_D^2(1-d) - \tfrac{1}{2}b + (1-b)\left\{W(-Q_D(b) + cb) + \tfrac{1}{2}u_D^2(b) + p_D(b)\right\}. \tag{A 19}$$

Assuming $Q(b) = 0$ and applying (2.16) at $y = b$, (A 19) becomes

$$c^2 = \int_b^d \left(u_D^2 - 2\eta u_D^2 + \eta^2\right)\mathrm{d}y + U_D^2(1-d) - b + 2(1-b)\left\{\tfrac{1}{2}u_D^2(b) - \eta(b)\right\}. \tag{A 20}$$

The potential vorticity equation (2.18) and the geostrophic equation (2.13) along with the pressure (2.16) are used to express (A 20) in terms of exact differentials:

$$c^2 = \frac{1}{W}\left[\tfrac{2}{3}u_D^3 - \eta u_D\right]_b^d + U_D^2(1-d) - b + 2(1-b)\left\{\tfrac{1}{2}u_D^2(b) - \eta(b)\right\}. \tag{A 21}$$

This is given as equation (3.4) in the main text.

https://doi.org/10.1017/S0022112004001351 Published online by Cambridge University Press

A.1.3. *Asymptotic solution as* $W \to 0$

It is important to confirm that as W approaches zero the governing equations reduce to those of the non-rotating case. Using the Maclaurin expansion for hyperbolic functions expressions (2.19) and (2.20) become

$$\eta(y) = \eta_0 + Wy\,u_0 \tag{A 22a}$$

and

$$u_D(y) = u_0 + Wy\eta_0 \tag{A 22b}$$

respectively. Applying (A 22a,b) at $y = 1$ gives

$$\eta(1) = \eta_0 + Wu_0 \tag{A 23a}$$

and

$$u_D(1) = u_0 + W\eta_0 \tag{A 23b}$$

Substituting (A 23a,b) into the continuity equation (3.3) gives

$$c = -u_0(1 - \eta_0) + O(W). \tag{A 24}$$

Substituting (A 23a,b) into the momentum equation (3.4) gives

$$c^2 = -2u_0^2\eta_0 + 2u_0^2 + \eta_0^2 - 2\eta_0 + O(W). \tag{A 25}$$

On substituting (A 23a,b) and making use of (A 25) the expression for energy loss (3.2) becomes

$$\Delta E = \eta_0 - \tfrac{1}{2}u_0^2 + O(W). \tag{A 26}$$

Now we compare the leading-order terms in the expressions above with the non-rotating governing equations described in § 2.1. The non-rotating expressions are non-dimensionalized and the notation used for the rotating theory is applied. The continuity equation becomes

$$c = -u_0(1 - \eta_0). \tag{A 27}$$

Hence (A 27) is equivalent to (A 24). The expression for the non-rotating conservation of momentum becomes

$$c^2 = -2u_0^2\eta_0 + 2u_0^2 + \eta_0^2 - 2\eta_0, \tag{A 28}$$

confirming that (A 28) is equivalent to (A 25). Finally rearranging (A 2) to give an expression for the non-rotating energy loss as a function of the downstream depth and velocity gives

$$\Delta E = \eta_0 - \tfrac{1}{2}u_0^2, \tag{A 29}$$

which is equivalent to (A 26). Therefore the rotating energy loss solution tends to the non-rotating solution as W tends to zero, while the energy-conserving version has $\eta_0 = \frac{1}{2}$, $u_0 = 1$ and $c = \frac{1}{2}$.

A.2. *Solution of the equations*

The general form of the main equations is given in § 3. In this section we give the detailed form and solution method for each of the three cases. We also derive equations to describe the transition points between the cases. The results are given in § 4.

https://doi.org/10.1017/S0022112004001351 Published online by Cambridge University Press

A.2.1. *Case A*

Governing equations for Case A

For case A the governing equations (3.2), (3.3) and (3.4) become:

energy loss

$$\Delta E = W^{-1}\left[-\tfrac{1}{3}u_D^3(1) + \tfrac{1}{2}\eta(1)u_D(1) + \tfrac{1}{3}u_0^3 - \tfrac{1}{2}\eta_0 u_0\right] - \tfrac{1}{2}c^2; \tag{A 30}$$

continuity

$$c = W^{-1}\left[\tfrac{1}{2}u_D^2(1) - \eta(1) + \eta_0 - \tfrac{1}{2}u_0^2\right]; \tag{A 31}$$

momentum

$$c^2 = W^{-1}\left[-\tfrac{2}{3}u_D^3(1) + \eta(1)u_D(1) + \tfrac{2}{3}u_0^3 - \eta_0 u_0\right] + u_0^2 - 2\eta_0. \tag{A 32}$$

The flow structure equations (2.19) and (2.20) for case A become

$$\eta(1) = \eta_0 \cosh W + u_0 \sinh W \tag{A 33}$$

and

$$u_D(1) = u_0 \cosh W + \eta_0 \sinh W \tag{A 34}$$

respectively. The momentum equation (A 32) is rearranged to give

$$0 = -\tfrac{2}{3}u_D^3(1) + \eta(1)u_D(1) + \tfrac{2}{3}u_0^3 - \eta_0 u_0 + W\left(u_0^2 - 2\eta_0 - c^2\right). \tag{A 35}$$

By substituting the continuity (A 31) and the flow structure equations (A 33) and (A 34), into (A 35) an equation as a function of u_0 with η_0 and W as constants is obtained. This is then solved using a numerical method (see below).

Transition point between cases A and B

In the energy loss solution the principle variables are a function of the two constants η_0 and W. As successive values of η_0 are considered for a particular level of rotation the depth at the left-hand wall, $\eta(1)$, will decrease until $\eta(1) = 0$, i.e. the transition point between cases A and B. Therefore, for every level of rotation for which the dissipationless geometry is that of case A, W_A, a transition will occur at some value of η_0. As W_A is increased the slope of the interface is greater and hence the transition will occur at larger values of η_0. To obtain the value of η_0 which coincides with the end-point of case A for each value of W_A, $\eta(1) = 0$ is substituted into (A 33), (A 34) and (A 31) to give

$$u_0 = -\eta_0 / \tanh W_A, \tag{A 36}$$

$$u_D(1) = -\eta_0 / \sinh W_A, \tag{A 37}$$

$$c = \frac{1}{W_A}\left[\eta_0 - \frac{\eta_0^2}{2\tanh^2 W_A} + \frac{\eta_0^2}{2\sinh^2 W_A}\right], \tag{A 38}$$

respectively. Substituting the above into (A 35) gives the momentum equation in terms of η_0, which is solved numerically to give the values shown in table 1. From table 1 it is apparent that for $W = 0.1$ the current fills the full width of the channel for all but very shallow depths $\eta_0 < 0.020$, whilst for $W = 0.67$ the case A geometry only occurs between the energy-conserving depth $\eta_0 = 0.685$ and $\eta_0 = 0.684$. The transition between case A and B in the energy-conserving solution occurs at $W = 0.671$.

Numerical solution for case A

The roots of (A 35) are obtained using the Newton–Raphson method. The first approximation is taken as the energy-conserving solution of u_0 for a particular value

https://doi.org/10.1017/S0022112004001351 Published online by Cambridge University Press

W	η_0	u_0	c
0.67	0.6842	−1.1697	0.6719
0.6	0.5686	−1.0588	0.6783
0.5	0.4166	−0.9016	0.6597
0.4	0.2813	−0.7405	0.6044
0.3	0.1663	−0.5710	0.5083
0.2	0.0770	−0.3904	0.3704
0.1	0.0198	−0.1987	0.1961

TABLE 1. Values of W, η_0, u_0 and c (to 4 decimal places) for the transition points between cases A and B.

of η_0 and W. The aim is to obtain a set of solutions for u_0 at successive values of η_0 for which $\eta(1)$ is positive, i.e. case A. η_0 is decreased in steps of 0.01. At each step a number of iterations are performed until u_0 converges to a solution. Generally a solution to 4 decimal places is obtained within 4 iterations. The initial approximation at each step is taken as the previous solution for u_0. The full solutions are plotted in § 4.

A.2.2. *Case B*

Governing equations for Case B

For case B the governing equations become

energy loss

$$\Delta E = W^{-1}\left[-\tfrac{1}{3}U_D^3 + \tfrac{1}{3}u_0^3 - \tfrac{1}{2}\eta_0 u_0\right] + \tfrac{1}{2}U_D^2(1-d) - \tfrac{1}{2}c^2; \tag{A 39}$$

continuity

$$c = W^{-1}\left[\tfrac{1}{2}U_D^2 + WU_D(1-d) + \eta_0 - \tfrac{1}{2}u_0^2\right]; \tag{A 40}$$

momentum

$$c^2 = W^{-1}\left[-\tfrac{2}{3}U_D^3 + \tfrac{2}{3}u_0^3 - \eta_0 u_0\right] + U_D^2(1-d) - 2\eta_0 + u_0^2. \tag{A 41}$$

The flow structure equations for case B become

$$\eta(d) = 0 = \eta_0 \cosh Wd + u_0 \sinh Wd \tag{A 42}$$

and

$$u_D(d) = U_D = u_0 \cosh Wd + \eta_0 \sinh Wd$$

(from 2.20) respectively. In the free stream $\eta = 0$, hence

$$d = W^{-1} \operatorname{arctanh}(-\eta_0/u_0)$$

(from A 42). The momentum equation (A 41) is rearranged to give

$$0 = -\tfrac{2}{3}U_D^3 + \tfrac{2}{3}u_0^3 - \eta_0 u_0 + WU_D^2(1-d) + W\left(u_0^2 - 2\eta_0 - c^2\right). \tag{A 43}$$

Transition between cases C and B

For the energy conserving solution the transition from case B to C occurs at $W = 1.898$ (to 3 decimal places). To obtain the dissipative solutions for case C ($1.898 \leqslant W \leqslant 3.0$) the value of η_0 is decreased from the respective energy-conserving value until $\eta_0 = 1$ and $b = 0$, i.e. the starting point of case B. To obtain the transition values $\eta_0 = 1$ is inserted into the flow structure equations (A 42), and the continuity

https://doi.org/10.1017/S0022112004001351 Published online by Cambridge University Press

W	η_0	u_0	d	c
3.0	1	−1.4108	0.2949	0.8684
2.9	1	−1.4109	0.3051	0.8641
2.8	1	−1.4110	0.3159	0.8596
2.7	1	−1.4112	0.3276	0.8547
2.6	1	−1.4113	0.3401	0.8495
2.5	1	−1.4115	0.3536	0.8439
2.4	1	−1.4118	0.3683	0.8379
2.3	1	−1.4121	0.3841	0.8314
2.2	1	−1.4125	0.4014	0.8244
2.1	1	−1.4129	0.4203	0.8167
2.0	1	−1.4135	0.4410	0.8084
1.9	1	−1.4142	0.4639	0.7993

TABLE 2. Values for W, η_0, u_0, d and c (to 4 decimal places) for the transition points between cases C and B.

equation (A 40) to give

$$u_0 = -1/\tanh W_A, \tag{A 44}$$

$$u_D(1) = -1/\sinh W_A, \tag{A 45}$$

$$c = \frac{1}{W}\left[\frac{1}{2} + \frac{W(1-d)}{\sinh Wd}\right], \tag{A 46}$$

respectively. Substituting the above into (A 41) enables the momentum equation to be expressed in terms of d and solved numerically, with the results given in table 2.

Numerical solution for case B

By substituting the continuity (A 40) and the flow structure equations given above into (A 43) an equation as a function of u_0 with η_0 and W as constants is obtained. This is solved using the same numerical method as for case A, with the exception that the first initial approximations for the solutions for $0 < W < 0.671$ are taken as the end-points of case A (table 1). For the range $0.671 < W < 1.898$ the energy-conserving values for case B are used. In the range $1.898 < W < 3.0$ the transition points between cases C and B are required (table 2).

A.2.3. *Case C*

Governing equations for case C

For case C the governing equations become

energy loss

$$\Delta E = \frac{1}{2(1-b)}\left\{\frac{1}{W}\left[-\tfrac{2}{3}U_D^3 + \tfrac{2}{3}u_D^3(b) - u_D(b)\right] + U_D^2(1-d) - b - c^2\right\}; \tag{A 47}$$

continuity

$$c = \frac{1}{W}\left[\tfrac{1}{2}U_D^2 + WU_D(1-d) + \eta(b) - \tfrac{1}{2}u_D(b)^2\right]; \tag{A 48}$$

momentum

$$c^2 = \frac{1}{W}\left[-\tfrac{2}{3}U_D^3 + \tfrac{2}{3}u_D(b)^3 - u_D(b)\right] + U_D^2(1-d) - 2 - u_D(b)^2 - bu_D(b)^2 + b. \tag{A 49}$$

https://doi.org/10.1017/S0022112004001351 Published online by Cambridge University Press

The flow structure equations for case C become

$$\eta(b) = 1 = \eta_0 \cosh Wb + u_0 \sinh Wb$$

(from 2.19) and

$$u_D(b) = u_0 \cosh Wb + \eta_0 \sinh Wb$$

(from 2.20) respectively. In the free-stream $\eta(d) = 0$, hence

$$d = W^{-1} \operatorname{arctanh}(-\eta_0/u_0)$$

(from 2.19) remains valid. Using the flow structure equations gives

$$Wd = \operatorname{arctanh}[(-u_0 \cosh Wb)^{-1} + \tanh Wb]. \tag{A 50}$$

The momentum equation is rearranged to give

$$0 = -\tfrac{2}{3}U_D^3 + \tfrac{2}{3}u(b)^3 - u_D(b) + WU_D^2(1-d) + W\{u_D(b)^2 - 2 - bu_D(b)^2 + b - c^2\}. \tag{A 51}$$

Numerical solution for Case C

By substituting the continuity (A 48) and the flow structure equations given above into the momentum equation (A 51) an equation as a function of b with η_0 and W as constants is obtained. This is solved using the numerical method described for case A, where the first approximations are taken as the energy-conserving solutions for b within the range $1.898 < W < 3.0$. The end-points of case C are listed in table 2. The full solutions for case C along with those for cases A and B are discussed in § 4.

REFERENCES

Benjamin, T. B. 1968 Gravity currents and related phenomena. *J. Fluid Mech.* **31**, 209–248.

Griffiths, R. W. 1986 Gravity currents in rotating systems. *Annu. Rev. Fluid Mech.* **18**, 59–89.

Hacker, J. N. 1996 Gravity currents in rotating channels. PhD thesis, University of Cambridge.

Hacker, J. N. & Linden, P. F. 2002 Gravity currents in rotating channels. Part 1. Steady-state theory. *J. Fluid Mech.* **457**, 295–324.

Lamb, H. 1932 *Hydrodynamics*, 6th edn. Cambridge University Press (Dover edition, 1945).

Lane-Serff, G. F., Beal, L. M. & Hadfield, T. D. 1995 Gravity current flow over obstacles. *J. Fluid Mech.* **292**, 39–53.

Martin, J. R., Smeed, D. A. & Lane-Serff, G. F. 2004 Rotating gravity currents. Part 2. Potential vorticity theory. *J. Fluid Mech.* **000**, 000–000.

Nof, D. 1987 Penetrating outflows and the dam breaking problem. *J. Mar. Res.* **45**, 557–577.

Rossby, C. G. 1938 On the mutual adjustment of pressure and velocity distributions in certain current systems. Part 2. *J. Fluid Mech.* **135**, 95–110.

Simpson, J. E. 1982 Gravity currents in the laboratory, atmosphere and ocean. *Annu. Rev. Fluid Mech.* **14**, 213–234.

Simpson, J. E. 1997 *Gravity Currents: in the Environment and in the Laboratory*, 2nd Edn. Cambridge University Press.

Stern, M. E. 1980 Geostrophic fronts, bores, breaking and blocking waves. *J. Fluid Mech.* **99**, 687–704.

Stern, M. E., Whitehead, J. A. & Hua, B. L. 1982 The intrusion of a density current along a coast of a rotating fluid. *J. Fluid Mech.* **123**, 237–265.

https://doi.org/10.1017/S0022112004001351 Published online by Cambridge University Press